

MACHINE LEARNING-ASSISTED PREDICTION OF THERMOPHYSICAL PROPERTIES OF NICKEL-BASE ALLOYS OVER A TEMPERATURE RANGE

Sudeepa Mondal^{1,2}, Nandana Menon¹, Asok Ray^{1,2}, and Amrita Basak^{1,*}

¹Department of Mechanical Engineering, The Pennsylvania State University,
University Park, PA 16802, USA

²Department of Mathematics, The Pennsylvania State University,
University Park, PA 16802, USA

* Communicating Author: aub1526@psu.edu

Abstract

Calculation of thermophysical properties of complex metallic alloys as functions of composition and temperature is essential to design new alloy systems that are suitable for advanced manufacturing processes such as additive manufacturing. Once the properties are obtained, they are typically integrated with a meso-scale simulation framework to understand the impact of composition on different properties. While the forward problem is straight forward, the inverse problem necessitates the integration of the thermodynamic and meso-scale modeling with an optimization framework. The usage of machine learning (ML) tools is, therefore, deemed to be conducive to the development of a digital twin framework for both thermodynamic as well as meso-scale modeling. This paper implements a Gaussian Process (GP) framework to predict thermophysical properties (e.g., bulk density, solidus/liquidus temperatures) of a nickel-base metallic alloy system, nickel-chromium-aluminum (Ni-Cr-Al), over a temperature range. The results show that the proposed GP-based framework is conducive to predicting thermophysical properties with good accuracy and, thus, can be implemented as a surrogate in the digital twin development of additive manufacturing processes.

Introduction

Nickel is a versatile element. It can be alloyed with many other critical elements in the periodic table to design high-performance material systems. Wide solubility ranges among iron, chromium, and nickel have facilitated the development of many critical components. The nickel-chromium-aluminum (Ni-Cr-Al) alloy is one such alloy that is extensively used in high-pressure devices for neutron scattering because of its high strength, low neutron attenuation, and non-magnetism at very low temperatures [1]. The typical composition used by the nuclear industries has 57.0 wt. % Ni, 40.0 wt. % Cr, and 3.0 wt. % Al, and is hardened by precipitation. For this specific composition, Cr dissolves completely in Ni at high temperatures and forms a supersaturated solid solution (Ni, Cr) after quenching. Aluminum (Al) typically aids in forming precipitates in nickel-base alloys facilitating material strengthening. Since the establishment of the International Nickel Company (Inco) in 1902, in addition to Al, Cu, Cr, and Fe, Ni has been alloyed with many other elements such as Boron (B), Carbon (C), Cobalt (Co), Hafnium (Hf), Molybdenum (Mo), Niobium (Nb), Rhenium (Re), Tantalum (Ta), and Titanium (Ti). Because of

the presence of multiple elements, nickel-base alloys demonstrate a melting range as opposed to a specific melting point exhibited by a pure element. The melting range is defined by the difference between the liquidus and the solidus temperatures. An accurate prediction of the solidus and liquidus temperatures and the melting range as a function of alloy composition over a temperature range is immensely critical to developing numerical simulation models for manufacturing processes such as additive manufacturing (AM) [2].

First-principle calculations using computational thermodynamics [3] are essential to obtain the necessary thermophysical properties. Once the properties are obtained, they are typically integrated with a meso-scale simulation framework such as flow-thermal or deformation modeling to understand the impact of composition on different properties such as the melt pool dimensions in case of flow-thermal modeling or yield stress in case of tensile deformation modeling [4]–[6]. While the forward problem is execution-friendly, the inverse problem is not. To find out the composition that would yield the desired property, the thermodynamic modeling software and the meso-scale modeling software need to be coupled with an optimization framework, which would be computationally near intractable [7]. The usage of machine learning (ML) tools is, therefore, deemed to be conducive to the development of a digital twin framework for both thermodynamic as well as meso-scale modeling. A significant amount of work has been performed in a supervised learning setting to predict material properties [8], [9]. However, most of the work has been focused on developing ML tools that provide point estimates for the quantities of interest. Since the deterministic ML methods cannot quantify the uncertainty of prediction [10], [11], it is desirable to replace the point estimates of the predicted values with a prediction probability through modeling the uncertainty in the dataset. To fulfill such a requirement, this paper presents a principled approach to data-driven modeling using a probabilistic ML framework.

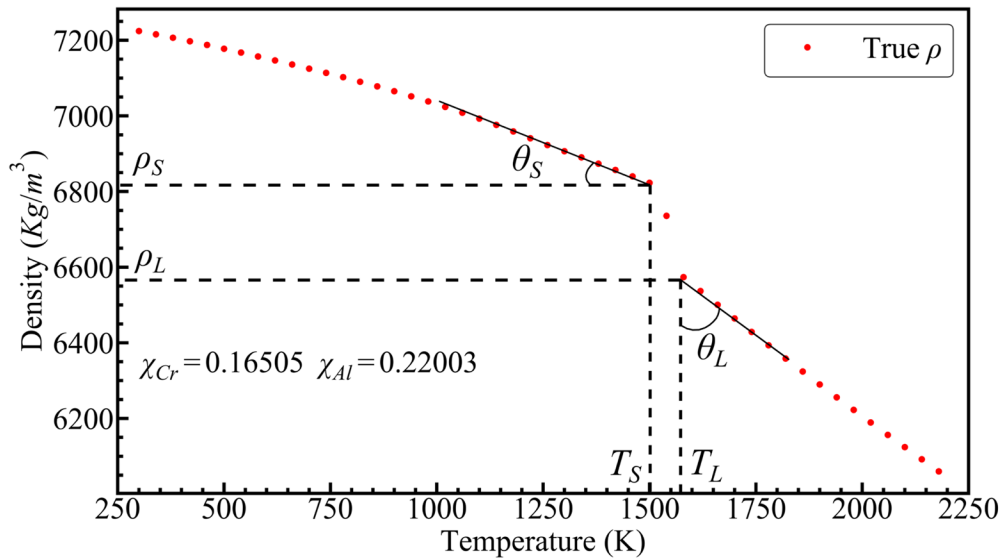


Figure 1. Variation of bulk density (ρ) as a function of temperature for Ni-Cr-Al alloy with $\chi_{Cr} = 0.16505$, $\chi_{Al} = 0.22003$ (balance = Ni). Solidus and liquidus temperatures and densities are marked with dashed lines. Here, χ is the weight fraction.

Gaussian Process (GP) [12] regression is utilized in this work to develop a Bayesian non-parametric surrogate [13] for predicting the relevant thermophysical properties as a function of temperature (T) for complex alloys, along with uncertainty quantification (UQ) [14] associated with these predictions. Ni-Cr-Al which shows a complex solidification behavior is selected as a candidate alloy, and its bulk density (ρ) is predicted by piece-wise GP surrogates. GP surrogates allow for probabilistic prediction of ρ as a function of temperature (T) in the solid and liquid phases separately, along with the prediction of estimated (i.e., mean) ρ and T at the solidus and liquidus properties. The nickel-base alloys typically show a continuous decrease in the density with temperature, followed by an abrupt discontinuity due to phase change which is followed by a continuous decrease as shown in Figure 1.

Methods

This subsection provides a brief overview of the surrogate development technique that is used as the foundation for the data-driven framework to predict the thermophysical properties. A few salient properties of GP surrogates are:

- GPs are stochastic processes that assume multivariate jointly Gaussian distribution for any finite collection of random variables.
- GPs being non-parametric models, do not assume predefined functional relationships between the inputs and outputs, thereby provide more flexibility in modeling complex nonlinear relationships.
- A GP surrogate being Bayesian tends to fit a surrogate that is neither too complex nor too simple.

The GP predictions are made via a posterior probability distribution, which is a normal distribution, fully specified by its mean and covariance. Such a probabilistic prediction inherently provides a measure of the prediction uncertainties through the variance of the distribution. Having a probabilistic estimate is also beneficial as it provides a confidence level to the predictions. For example, if the function $f(\mathbf{x})$ for an input \mathbf{x} is considered a random variable, then, for a finite sub-collection $\{\mathbf{x}_1, \mathbf{x}_2, \dots, \mathbf{x}_N\}$, the corresponding function outputs $\{f(\mathbf{x}_1), f(\mathbf{x}_2), \dots, f(\mathbf{x}_N)\}$ are assumed to have a multivariate jointly Gaussian distribution completely characterized by a mean function and a covariance function. Let $D^{trn} = \{(\mathbf{x}_i^{trn}, y_i^{trn})\}, i = 1, \dots, N$, be the training set that are available for model formulation, then the regression model is assumed to be,

$$y_i^{trn} = f(\mathbf{x}_i^{trn}) + \varepsilon_i \quad (1)$$

Here, the additive noise ε_i are independent and identically distributed zero-mean Gaussian random variables, i.e., $\varepsilon_i \sim \mathcal{N}(0, \sigma^2)$. On incorporating the noise term, the joint distribution of the observed values and the functional values at the test locations are

$$\begin{bmatrix} \mathbf{y}^{trn} \\ \mathbf{y}^{tst} \end{bmatrix} \sim \mathcal{N} \left(0, \begin{bmatrix} k(\mathbf{x}^{trn}, \mathbf{x}^{trn}) + \sigma^2 I & k(\mathbf{x}^{trn}, \mathbf{x}^{tst}) \\ k(\mathbf{x}^{tst}, \mathbf{x}^{trn}) & k(\mathbf{x}^{tst}, \mathbf{x}^{tst}) \end{bmatrix} \right) \quad (2)$$

where $D^{tst} = \{(\mathbf{x}_i^{tst}, y_i^{tst})\}$ is the test set in which y^{tst} is the output at \mathbf{x}^{tst} which is the unknown variable. $k(\cdot)$ is the covariance function. By the property of multivariate normal distributions, the conditional distribution of the outputs at the test location is also Gaussian.

$$\mathbf{y}^{tst} | \mathbf{y}^{trn}, \mathbf{x}^{trn}, \mathbf{x}^{tst} \sim \mathcal{N}(\mu^{tst}, \Sigma^{tst}) \quad (3)$$

Here,

$$\mu^{tst} = K(\mathbf{x}^{tst}, \mathbf{x}^{trn}) [K(\mathbf{x}^{trn}, \mathbf{x}^{trn}) + \sigma^2 I]^{-1} \mathbf{y}^{trn} \quad (4)$$

$$\Sigma^{tst} = K(\mathbf{x}^{tst}, \mathbf{x}^{tst}) - K(\mathbf{x}^{tst}, \mathbf{x}^{trn}) [K(\mathbf{x}^{trn}, \mathbf{x}^{trn}) + \sigma^2 I]^{-1} K(\mathbf{x}^{trn}, \mathbf{x}^{tst})$$

$K(\cdot)$ is the covariance kernel. The GP predictions are made via the posterior probability distribution, which is a normal distribution, fully specified by its mean, μ^{tst} , and covariance, Σ^{tst} . Such a probabilistic prediction inherently provides a measure of the prediction uncertainties through the variance of the distribution. Having a probabilistic estimate is also beneficial as it provides with a confidence level of the predictions.

The thermophysical properties, such as thermal conductivity (k), bulk density (ρ), specific heat (C_p), and thermal diffusivity (D), typically show a discontinuity across the solidus-liquidus mushy zone (defined as the temperature interval where the solid and liquid phases co-exist) for multi-component complex alloys such as Ni-Cr-Al. Figure 1 shows the variation of ρ as a function of temperature in the range of 300 K to 2200 K for a Ni-Cr-Al alloy with the elemental composition (in wt. %) $\chi_{Cr} = 0.16505$, $\chi_{Al} = 0.22003$ (balance = Ni). Here, χ is the weight fraction. It shows near-linear variations of ρ in the solid and liquid phases, with a sharp change in the vicinity of the solidus (T_S) and liquidus (T_L) temperatures. To formulate the ML models for predicting $\rho(T)$ at different compositions for alloys that show such behavior, a linearity assumption is made for the nature of variation of $\rho(T)$ in the solid and liquid phases. This assumption follows from the observations of very weak non-linearity in the temperature dependency of density variations widely used in metallic alloys. The linearity assumptions can be relaxed for alloys showing non-linear behavior by learning the functional relationship of $\rho(T)$ in the solid and liquid phases individually. However, such a learning procedure would require additional model complexities and the associated computational expenses of learning such a function over a wide range of temperatures in the solid and liquid phases. The proposed prediction problem involves learning GP models for the following six outputs for given inputs in Ni-Cr-Al composition space:

- (a) solidus temperature (T_S)
- (b) liquidus temperature (T_L)
- (c) solidus density (ρ_S)
- (d) liquidus density (ρ_L)
- (e) mean slope $\left(\frac{\partial \rho(T)}{\partial T}\right)$ of $\rho(T)$ in the solid phase (θ_S) and,
- (f) mean slope $\left(\frac{\partial \rho(T)}{\partial T}\right)$ of $\rho(T)$ in the liquid phase (θ_L).

If the first four output variables (a) to (d) are predicted satisfactorily, the mean slopes (e) and (f) would provide the piecewise density variation as a function of temperature in the solid and liquid phases, respectively (based on the assumption of linearity). This piecewise modeling

formulation, therefore, directly allows the end-users to have estimates of the temperatures and properties at solidus and liquidus for an unknown composition by learning the respective relationships in the input space of compositions. The density in the mushy liquidus-solidus zone is approximated by linear interpolation between the points (T_S, ρ_S) and (T_L, ρ_L) . Since it is desirable to design surrogates without the requirement of a huge volume of data, the effect of the size of the training set on the prediction accuracy has been studied. For this, variable training set sizes ranging from 10 to 100, in intervals of 10, have been explored. Each training set has been selected as Latin Hypercube Samples (LHS) in the design space: $(\chi_{Cr}, \chi_{Al}, T)$ are generated with $\chi_{Cr} \in [10^{-4}, 0.33]$, $\chi_{Al} \in [10^{-4}, 0.33]$, $T \in [300, 2200]$ K. A test set of 100 randomly selected: (χ_{Cr}, χ_{Al}) combinations is set aside for testing the performance of the GP surrogate. The output at each input point is a scalar: ρ (kg/m^3), which is treated as the true density (i.e., the ground truth), for each input condition, as obtained from simulations in the software Thermo-Calc 2020a [15].

Results and discussion

Impact of Training Data Size

Typically for any ML method, the prediction performance improves as the amount of training data increases. However, for practical problems, training data procurement can be a challenge. On the other hand, GPs are $\mathcal{O}(N^3)$ in computational complexity [12], bottlenecked by the $N \times N$ matrix inversion, implying that large training data sizes would result in more computational time for training GP surrogates. Hence, when possible, it is necessary to find an appropriate training data size for efficient training of the GP surrogates. This subsection shows how the training size affects the prediction performance of the GPs. The metrics chosen for evaluating the performance of the GPs are:

- (a) Normalized L_2 error (ϵ): It is the ratio of the Euclidean norm of the error of the predictive posterior GP mean of an output (\hat{y}_μ) and the Euclidean norm of the true value of the output (y^*), i.e. $\epsilon = \frac{\|\hat{y}_\mu - y^*\|_2}{\|y^*\|_2}$, calculated on the total test set.
- (b) R^2 score: It is the Coefficient of Determination assessing the degree to which the posterior GP mean of output compares with the respective true values, calculated on the total test set.
- (c) Normalized standard deviation of prediction ($\bar{\sigma}$): It is the total standard deviation of the predictive GP posterior over the test points, scaled with a factor σ_{max} such that $\bar{\sigma} \in [0,1]$.
- (d) $\alpha(\pm 2\sigma)$: Corresponds to the percentage of the cases for which the true values of the outputs lie within the 95% confidence interval of the predictive GP posterior distributions at the test locations

Figure 2 shows the variation of ϵ and $\bar{\sigma}$ as a function of the training data size for the six outputs. It is observed that both ϵ and $\bar{\sigma}$ have a decreasing trend as more training data is utilized in the initial GP learning phase. For all the six outputs, ϵ nearly saturates when the training data size is 70, which is also when $\bar{\sigma}$ saturates for all outputs except θ_S and θ_L . It is desirable to choose a training data size that not only results in low ϵ (more accurate mean predictions), but also low $\bar{\sigma}$ (less uncertainty in prediction). The normalizing scale σ_{max} in defining $\bar{\sigma}$ has been chosen as the total standard deviation of prediction using the minimum training data size of 10. Hence, with the

addition of training points, a reduction in $\bar{\sigma}$ denotes a reduction in the total prediction uncertainty. In this work, a consistent training size of 70 has been chosen for prediction across all the outputs. Although $\bar{\sigma}$ for θ_S and θ_L is not as low as the rest of the outputs, there is still at least a 50% reduction in prediction uncertainty

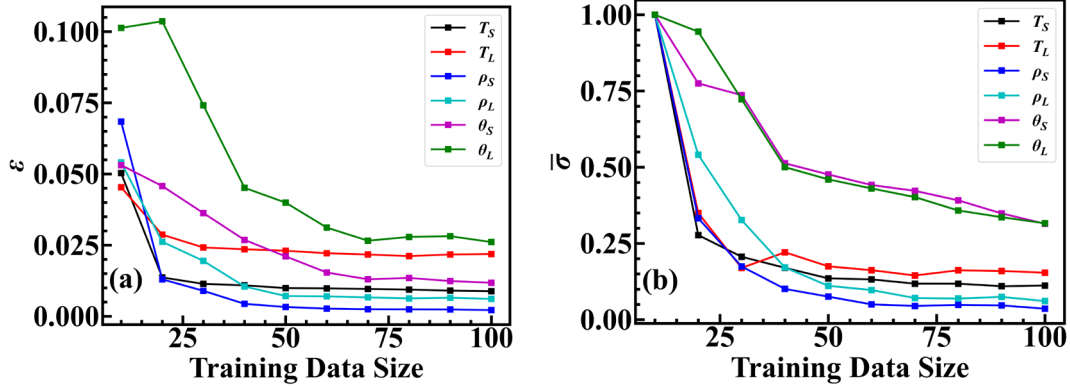


Figure 2. Variation of (a) ϵ and (b) $\bar{\sigma}$ over the test set as a function of training data size for the six outputs of interest.

Density Predictions by GPs

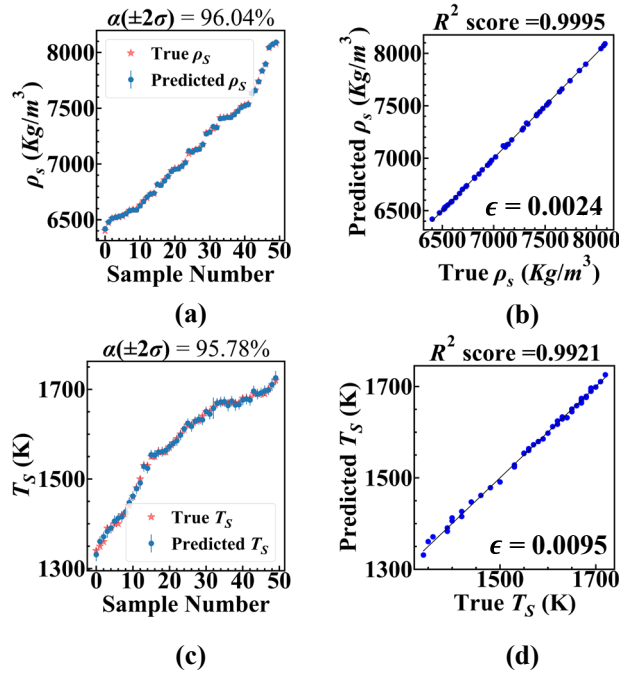


Figure 3. Probabilistic predictions of (a) T_S and (c) ρ_S in a subset of the test set compared with the respective true values. Parity plots comparing the true (b) T_S and (d) ρ_S at the test points with the corresponding mean predicted values.

The performance of the proposed algorithm is illustrated in Figure 3, whereby the predictions of T_S and ρ_S are compared with their corresponding true values for 50 randomly selected test points out of the total test set of points. Figures 3(a) and (c) show the probabilistic predictions, and Figures 3(b) and (d) show the parity plots comparing $\hat{T}_{S\mu}$ and $\hat{\rho}_{S\mu}$ with their respective true values. In Figures 3 (a) and (c), the X-axes correspond to the sample numbers (1 to 50) which are arranged in ascending order of their true values (T_S and ρ_S respectively). The predicted outputs at the corresponding test points are denoted as blue dots with error bars. The blue dots correspond to the mean ($\hat{T}_{S\mu}$) of the posterior predicted Gaussian distribution of T_S in Figures 3 (a) and mean ($\hat{\rho}_{S\mu}$) of the posterior predicted Gaussian distribution of ρ_S in Figures 3 (c). The error bars at each predicted point correspond to $\pm 2\sigma$ band of the respective Gaussian distributions. The metrics for the other outputs are tabulated in Table 1. An $\epsilon \leq 3\%$ is observed for almost all the predicted outputs, which is reflected in the high R^2 score for the output predictors. The $\pm 2\sigma$ band coverage varies between 94% - 98%, indicating that the variability of the outputs can be well explained by the GP models.

Table 1. Performance metrics for the predicted outputs: T_S , ρ_S , T_L , ρ_L , θ_S , θ_L

Output	ϵ	$\alpha(\pm 2\sigma)$	R^2 score
T_S	0.0095	95.78 %	0.9921
ρ_S	0.0024	96.04%	0.9995
T_L	0.0216	97.82%	0.9852
ρ_L	0.0066	96.51%	0.9953
θ_S	0.0129	94.00%	0.9988
θ_L	0.0265	97.49%	0.9873

Effects of Composition

The GP surrogate is employed to predict T_S , ρ_S , T_L , ρ_L , along with the mean gradients of $\rho(T)$ in the solid and liquid phases. The surrogate predictions are shown on the (χ_{Cr}, χ_{Al}) plane in Figure 4. The change in χ_{Cr} and χ_{Al} is observed to affect the solidus properties more except for the gradient in the liquid phase. The predictions indicate that with a decrease in χ_{Cr} and χ_{Al} there is a distinct increase of solidus and liquidus temperatures and densities, which is expected because of the increasing χ_{Ni} . Moreover, there is a noticeable increase in $\left| \frac{\partial \rho(T)}{\partial T} \right|$ with a decrease in χ_{Cr} and χ_{Al} , which indicates a steeper reduction of density as a function of temperature both in the solid and the liquid phases. However, there appears to be a thin band of alloy compositions near the higher end of χ_{Cr} and χ_{Al} (near top right corner of Figure 4 (f)) where $\left| \frac{\partial \rho(T)}{\partial T} \right|$ is higher than the neighboring compositions. Such a discontinuity in the trend is also observed in the T_L predictions (Figure 4 (b)). This discontinuity is confirmed in literature where T_L decreases with Ni % up until a certain value and then increases [16].

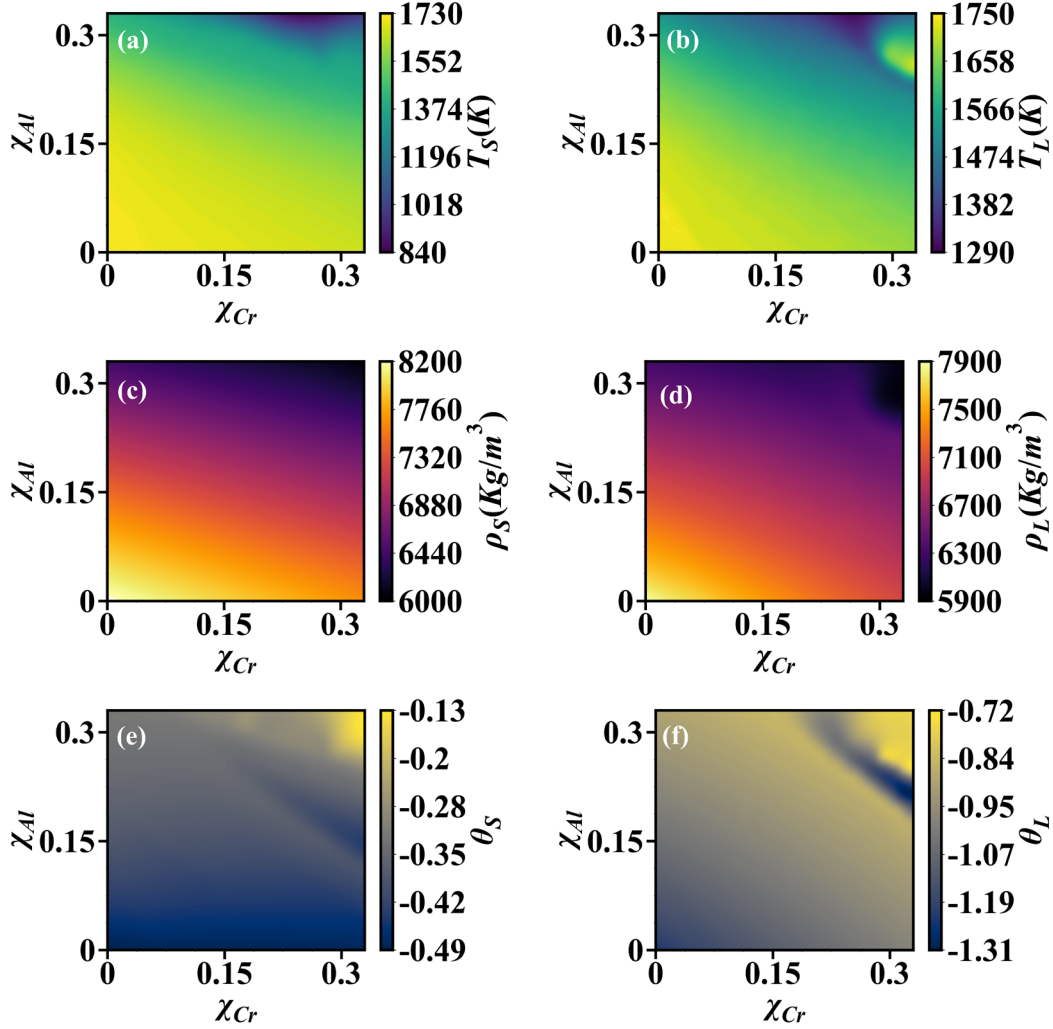


Figure 4. GP predictions of T_S (a), T_L (b), ρ_S (c), ρ_L (d), θ_S (e) and θ_L (f) shown on (χ_{Cr}, χ_{Al}) plane (balance = Ni).

Conclusion

This paper presents a machine learning (ML)-based framework for predicting variations of bulk density (ρ) of Ni-Cr-Al alloys as a function of temperature. The proposed framework is built upon Gaussian process (GP) modeling, which directly provides probabilistic estimates of the solidus and liquidus entities: T_S, ρ_S, T_L, ρ_L , along with the mean gradients of $\rho(T)$ in the solid and liquid phases. Although the demonstration is performed with the prediction of ρ , a similar approach can be adopted for the prediction of other thermophysical properties of interest. The GP model produces a normalized L_2 error (ϵ) less than 0.03 for all variables. With such prediction accuracy, the developed approach can accelerate the pace of material discovery by identifying novel materials with desired properties via an integrated computational materials engineering (ICME) approach, especially for the current state-of-the-art manufacturing processes such as additive manufacturing (AM) [8] and metamorphic manufacturing [9]. Once short-listed

compositions are obtained, further validation needs to be done with the computational thermodynamics approach for verification purposes.

Acknowledgments

The authors are thankful to Dr. James Rule of Thermo-Calc Software Inc. for generously providing technical support in generating the thermophysical property database of Ni-Cr-Al alloys. The work reported in this paper is supported in part by the Department of Mechanical Engineering at the Pennsylvania State University, University Park, PA 16802, and in part by the U.S. Army Engineer Research and Development Center through Contract Number W912HZ21C0001. Nandana Menon would like to acknowledge the James E. Marley Fellowship and the Kulakowski Travel Grant awarded by the Mechanical Engineering Department of the Pennsylvania State University and, the National Science Foundation Student Support offered by the organizing committee of the Solid Freeform Fabrication Symposium. Any opinions, findings, and conclusions in this paper are those of the authors and do not necessarily reflect the views of the supporting institutions

References

- [1] Y. Cheng *et al.*, “Ni–Cr–Al Alloy for neutron scattering at high pressures,” *Mater. Sci. Technol.*, vol. 36, no. 9, pp. 949–954, Jun. 2020.
- [2] A. Basak, R. Acharya, and S. Das, “Additive Manufacturing of Single-Crystal Superalloy CMSX-4 Through Scanning Laser Epitaxy: Computational Modeling, Experimental Process Development, and Process Parameter Optimization,” *Metall. Mater. Trans. A*, vol. 47, no. 8, pp. 3845–3859, 2016.
- [3] S. D. Meredith, J. S. Zuback, J. S. Keist, and T. A. Palmer, “Impact of composition on the heat treatment response of additively manufactured 17–4 PH grade stainless steel,” *Mater. Sci. Eng. A*, vol. 738, pp. 44–56, 2018.
- [4] R. Rettig and R. F. Singer, “Fast interpolation algorithm for the calculation of thermodynamic property maps of microstructures,” *Model. Simul. Mater. Sci. Eng.*, vol. 22, no. 8, p. 085002, Oct. 2014.
- [5] R. Rettig, N. C. Ritter, H. E. Helmer, S. Neumeier, and R. F. Singer, “Single-crystal nickel-based superalloys developed by numerical multi-criteria optimization techniques: design based on thermodynamic calculations and experimental validation,” *Model. Simul. Mater. Sci. Eng.*, vol. 23, no. 3, p. 035004, Mar. 2015.
- [6] R. Jha, N. Chakraborti, D. Diercks, A. Stebner, and C. V. Ciobanu, “Combined Machine Learning and CALPHAD Approach for Discovering Processing-Structure Relationships in Soft Magnetic Alloys,” *Comput. Mater. Sci.*, vol. 150, pp. 202–211, Oct. 2017.
- [7] S. Mondal, D. Gwynn, A. Ray, and A. Basak, “Investigation of Melt Pool Geometry Control in Additive Manufacturing Using Hybrid Modeling,” *Metals*, vol. 10, no. 5, 2020.
- [8] S. Chibani and F.-X. Coudert, “Machine learning approaches for the prediction of materials properties,” *APL Mater.*, vol. 8, no. 8, p. 80701, Aug. 2020.
- [9] Y. Sargam, K. Wang, and I. H. Cho, “Machine learning based prediction model for thermal conductivity of concrete,” *J. Build. Eng.*, vol. 34, p. 101956, 2021.
- [10] S. K. Kauwe, J. Graser, A. Vazquez, and T. D. Sparks, “Machine Learning Prediction of Heat Capacity for Solid Inorganics,” *Integr. Mater. Manuf. Innov.*, vol. 7, no. 2, pp. 43–51, 2018.

- [11] A. Y.-T. Wang, S. K. Kauwe, R. J. Murdock, and T. D. Sparks, “Compositionally restricted attention-based network for materials property predictions,” *npj Comput. Mater.*, vol. 7, no. 1, p. 77, 2021.
- [12] C. E. Rasmussen, “Gaussian processes in machine learning,” in *Summer school on machine learning*, 2003, pp. 63–71.
- [13] S. J. Gershman and D. M. Blei, “A tutorial on Bayesian nonparametric models,” *J. Math. Psychol.*, vol. 56, no. 1, pp. 1–12, 2012.
- [14] K. P. Murphy, *Machine learning: a probabilistic perspective*. MIT press, 2012.
- [15] J.-O. Andersson, T. Helander, L. Höglund, P. Shi, and B. Sundman, “Thermo-Calc & DICTRA, computational tools for materials science,” *Calphad*, vol. 26, no. 2, pp. 273–312, 2002.
- [16] M. Adachi, A. Sato, S. Hamaya, M. Ohtsuka, and H. Fukuyama, “Containerless measurements of the liquid-state density of Ni–Al alloys for use as turbine blade materials,” *SN Appl. Sci.*, vol. 1, no. 1, pp. 1–7, Jan. 2019.